

Radiometric Compensation using Stratified Inverses

Tian-Tsong Ng, Ramanpreet S. Pahwa, Jiamin Bai, Tony Q.S. Quek
Institute for Infocomm Research
Singapore

{ttng, rspahwa, jbai, qsquek}@i2r.a-star.edu.sg

Kar-Han Tan
HP Labs
Palo Alto, US

kar-han.tan@hp.com

Abstract

Through radiometric compensation, a projector-camera system can project a desired image onto a non-flat and non-white surface. This can be achieved by computing the inverse light transport of a scene. A light transport matrix is in general large and on the order of $10^6 \times 10^6$ elements. Therefore, computing the inverse light transport matrix is computationally and memory intensive. Two prior methods were proposed to simplify matrix inversion by ignoring scene inter-reflection between individual or clusters of camera pixels. However, compromising scene inter-reflection in spatial domain introduces spatial artifacts and how to systematically adjust the compensation quality is not obvious. In this work, we show how scene inter-reflection can be systematically approximated by stratifying the light transport of a scene. The stratified light transport enables a similar stratification in the inverse light transport. We can show that the stratified inverse light transport converges to the true inverse. For radiometric compensation, the set of stratified inverse light transport provides a systematic way of quantifying the tradeoff between computational efficiency and accuracy. The framework of stratified matrix inversion is general and can have other applications, especially for applications that involve large-size sparse matrices.

1. Introduction

A projector can be considered as a programmable light source that is able to control the appearance of a scene. When the ambient illumination can be ignored, the scene appearance as observed by a camera is a function of the projector pixel intensity. This function is linear due to the linear property of scene reflectance. The mapping between the projector pixels and the camera pixels is known as *light transport matrix*, the structure of which is determined by the scene. The inverse of the mapping (i.e., matrix inverse) tells us what should be the projector input if we specify a particular scene appearance from the camera viewpoint. The process of deriving the projector input given a desired scene

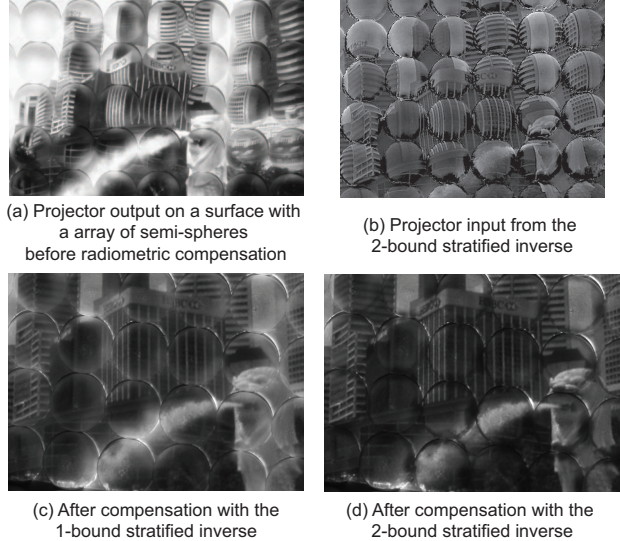


Figure 1. An illustration of radiometric compensation with stratified inverses on a complex scene with an array of semi-spheres.

appearance is referred as *view projection* [8] or *radiometric compensation* [9]. Fig. 1 shows an action of radiometric compensation. When a normal image is projected onto a surface with an array of semi-spheres, the city-scene image is distorted as the straight lines become curved. After radiometric compensation, the structures of the city scene is restored in the projected image.

In prior works, a light transport mapping was often modeled by a one-to-one mapping between the projector and camera pixels [4, 1, 3]. Although the inversion of such mapping is trivial, the one-to-one mapping can neither capture the global illumination effects such as inter-reflection, refraction, and scattering in the scene nor compensate for them. When the light transport mapping is modeled by a light transport matrix, the global illumination effects are captured. A light transport matrix has a dimension of the number of camera pixels by the number of projector pixels, which is in general large and on the order of $10^6 \times 10^6$ elements. Although a light transport matrix is in generally sparse, computing its inverse is computationally intractable. In [2, 8], a constraint known as the *display constraint* was

introduced to restrict the response of a camera pixel to only a projector pixel. The constraint ignores inter-reflection in the scene although it simplifies matrix inversion significantly by making the light transport matrix highly sparse and column-orthogonal. As a result, this method cannot effectively compensate for global illumination effects. In [9], a light transport is simplified by clustering the links between projector and camera pixels into independent clusters. Given these independent partitions, matrix inversion is computed separately for each cluster with a manageable size. This spatial clustering method ignores inter-reflection between clusters and can introduce spatial artifacts.

Both methods in [8, 9] compromises scene inter-reflection in spatial domain in order to make matrix inversion manageable. However, a systematic way for adjusting the quality of radiometric compensation in such methods is not obvious. In this work, we show how scene inter-reflection can be systematically approximated by stratifying the light transport of a scene. The stratified light transport enables a similar stratification in the inverse light transport. We can show that the stratified inverse light transport converges to the true inverse. For radiometric compensation application, the set of stratified inverse light transport provides a systematic way of quantifying the tradeoff between computational efficiency and accuracy. The framework of stratified matrix inversion is general and can have other applications. Stratified inverse computation mainly involves matrix multiplication and is particularly efficient for large-size sparse matrices. In Sec. 2, we formulate the problem of radiometric compensation. The inter-reflection cancellation operator introduced in [6] enables us to stratify a light transport as shown in Sec. 3, which in turn leads to a set of stratified inverse light transport as described in Sec. 4. We validate stratified inverses through simulations in Sec. 5 and experiments in Sec. 6. Finally, we conclude in Sec. 7.

2. Problem Formulation

In a projector-camera setup, a projector input image \mathbf{p} is projected onto a scene and captured by a camera as an image \mathbf{c} . Both \mathbf{p} and \mathbf{c} can, respectively, be represented as a vector of length N_p and N_c . As a projector can only take a non-negative input, hence $\mathbf{p} \in \mathbb{R}_+^{N_p}$ with \mathbb{R}_+^N denoting the non-negative orthant:

$$\mathbb{R}_+^N = \{\mathbf{x} \in \mathbb{R}^N \mid x_i \geq 0, i = 1, \dots, N\}. \quad (1)$$

In vector form, \mathbf{p} and \mathbf{c} are linearly related through a light transport matrix \mathbf{T} as in the forward-light-transport equation below [8, 9]:

Definition 1 (Forward Light Transport). *Given a light transport matrix $\mathbf{T} \in \mathbb{R}_+^{N_c \times N_p}$ and a projector input im-*

age $\mathbf{p} \in \mathbb{R}_+^{N_p}$, the camera image is given by:

$$\mathbf{c} = \mathbf{T}\mathbf{p}, \quad (2)$$

where $\mathbf{c} \in \mathbb{S}_c \subseteq \mathbb{R}_+^{N_c}$. \mathbb{S}_c is the column space of \mathbf{T} .

If the scene is complex in geometry, the camera image \mathbf{c} can be distorted and becomes not as comprehensible as the projector input image \mathbf{p} as shown in Fig. 1. To make \mathbf{c} comprehensible, we may want to specify \mathbf{c} and compute a non-negative \mathbf{p} that can best produce such \mathbf{c} . This is achievable given the inverse light transport mapping which is specified by the inverse light transport matrix \mathbf{T}^{-1} :

Definition 2 (Radiometric Compensation). *If the inverse light transport matrix $\mathbf{T}^{-1} \in \mathbb{R}^{N_p \times N_c}$ exists with $\mathbf{T}^{-1}\mathbf{T} = \mathbf{I}$, given a desired \mathbf{c} denoted as $\mathbf{c}_{desired} \in \mathbb{R}_+^{N_c}$, we can produce a camera image \mathbf{c}_{actual} as:*

$$\mathbf{c}_{actual} = \mathbf{T}f_+(\mathbf{T}^{-1}\mathbf{c}_{desired}), \quad (3)$$

where f_+ maps a vector to a feasible projector input image in $\mathbb{R}_+^{N_p}$, $\mathbf{c}_{desired} \in \mathbb{R}_+^{N_c}$, and $\mathbf{c}_{actual} \in \mathbb{S}_c \subseteq \mathbb{R}_+^{N_c}$.

The significance of the function f_+ in Definition 2 was not discussed in [8, 9]. In [8], the computed \mathbf{p} is always non-negative after simplifying \mathbf{T} to be column-orthogonal, while in [9] the negative values of the computed \mathbf{p} are treated as nuisance and clamped to zero in the graphic processing unit (GPU). We can show that the method adopted in [8] is equivalent to imposing a non-negativity constraint on \mathbf{p} , and the L_2 error between $\mathbf{c}_{desired}$ and \mathbf{c}_{actual} obtained by the method in [9] achieves a lower bound if \mathbf{T}^{-1} exists. The details of these results can be found [5].

3. Stratified Light Transport

The light observed by a camera \mathbf{L}_{out} could be an aggregate of light of multiple bounces originating from the light sources:

$$\mathbf{L}_{out} = \sum_{i=1}^{\infty} \mathbf{L}_{out}^{(i)}, \quad (4)$$

where $\mathbf{L}_{out}^{(n)}$ represents the n th-bounce light. In [6], an *inter-reflection cancellation operator* $\mathbf{C}^{(1)}$ was introduced. It was shown in [6] that the first-bounce light transport matrix can be obtained from the full light transport matrix \mathbf{T} through $\mathbf{C}^{(1)}$:

$$\mathbf{T}^{(1)} = \mathbf{C}^{(1)}\mathbf{T}. \quad (5)$$

Eq. 5 provides a way to compute $\mathbf{C}^{(1)}$ with $\mathbf{C}^{(1)} = \mathbf{T}^{(1)}\mathbf{T}^{-1}$. It was further shown in [6] that the unobserved n th-bounce light $\mathbf{L}_{out}^{(n)}$ can also be extracted from \mathbf{L}_{out} by using $\mathbf{C}^{(1)}$:

$$\mathbf{L}_{out}^{(n)} = \mathbf{C}^{(n)}\mathbf{L}_{out}, \quad (6)$$

where $\mathbf{C}^{(n)} = \mathbf{C}^{(1)}(\mathbf{I} - \mathbf{C}^{(1)})^{n-1}$.

Eq. 6 indicates that by knowing $\mathbf{T}^{(1)}$ and \mathbf{T} the contribution of different light bounces in light transport can be extracted. This observation suggests that we can simplify a light transport matrix by light bounce stratification. A light transport matrix \mathbf{T} transforms the input light field from light sources into the output light field observed by a camera:

$$\mathbf{L}_{out} = \mathbf{T}\mathbf{L}_{in}. \quad (7)$$

We define a stratified light transport matrix $\mathbf{T}^{(n)}$ as one that produces an output light field $\mathbf{A}_{out}^{(n)}$ with up to n th-bounce of light, where $\mathbf{A}_{out}^{(n)}$ is given by:

$$\mathbf{A}_{out}^{(n)} = \sum_{i=1}^n \mathbf{L}_{out}^{(i)} \doteq \mathbf{T}^{(n)}\mathbf{L}_{in}, \quad (8)$$

with $\mathbf{A}_{out}^{(1)} = \mathbf{L}_{out}^{(1)}$ and $\mathbf{A}_{out}^{(\infty)} = \mathbf{L}_{out}$.

By substituting $\mathbf{L}_{out}^{(i)} = \mathbf{C}^{(i)}\mathbf{L}_{out}$ and $\mathbf{L}_{out} = \mathbf{T}\mathbf{L}_{in}$ from Eq. 6 and 7 into Eq. 8, we obtain

$$\mathbf{T}^{(n)} = \left(\sum_{i=1}^n \mathbf{C}^{(i)} \right) \mathbf{T}. \quad (9)$$

We can show that Eq. 9 can be rewritten in terms of $\mathbf{T}^{(1)}$ and \mathbf{T} as shown in Proposition 1:

Proposition 1 (n -bounce Light Transport Matrix). *The n -bounce light transport matrix can be written as:*

$$\mathbf{T}^{(n)} = \left(\sum_{i=1}^n \binom{n}{i} (-\mathbf{T}^{(1)}\mathbf{T}^{-1})^{i-1} \right) \mathbf{T}^{(1)}, \quad (10)$$

where \mathbf{T}^{-1} is the inverse of the complete light transport matrix \mathbf{T} and $\binom{n}{i}$ is the binomial coefficients.

Proof. Substituting $\mathbf{C}^{(n)} = \mathbf{C}^{(1)}(\mathbf{I} - \mathbf{C}^{(1)})^{n-1}$ into Eq. 9, we obtain:

$$\mathbf{T}^{(n)} = \mathbf{C}^{(1)} \left(\sum_{i=1}^n (\mathbf{I} - \mathbf{C}^{(1)})^{i-1} \right) \mathbf{T}. \quad (11)$$

Note that the summation factor of Eq. 11 is a geometric series and it can be simplified as:

$$\sum_{i=1}^n (\mathbf{I} - \mathbf{C}^{(1)})^{i-1} = (\mathbf{C}^{(1)})^{-1} \left(\mathbf{I} - (\mathbf{I} - \mathbf{C}^{(1)})^n \right). \quad (12)$$

Substituting Eq. 12 into Eq. 11, we obtain:

$$\mathbf{T}^{(n)} = \left(\mathbf{I} - (\mathbf{I} - \mathbf{C}^{(1)})^n \right) \mathbf{T}. \quad (13)$$

Through binomial expansion and by substituting $\mathbf{C}^{(1)} = \mathbf{T}^{(1)}\mathbf{T}^{-1}$ [6] into Eq. 13, we obtain Eq. 10. \square

4. Stratified Matrix Inverses

From the stratified light transport obtained in Sec. 3, the inverse light transport can be similarly stratified and expressed as a linear function of the full light transport matrix \mathbf{T} and the 1-bounce light transport matrix $\mathbf{T}^{(1)}$.

In Proposition 2 we show that, for a scene with a maximum of N th-bounce light, we have $\mathbf{T}^{(i)} = \mathbf{T}^{(N)}$ if $i > N$. Hence, in this case, $\mathbf{T} = \mathbf{T}^{(N)}$.

Proposition 2 (Limit for Light Transport Matrix). *For a scene with at most N th-bounce light, $\mathbf{T}^{(M)} = \mathbf{T}^{(N)}$ if $M > N$.*

Proof. For a scene with at most N th-bounce light, $\mathbf{L}_{out}^{(M)}$ with $M > N$ would be 0, and the corresponding $\mathbf{C}^{(M)}$ will be zero. As a result, we can write Eq. 9 as

$$\mathbf{T}^{(n)} = \left(\sum_{i=1}^{\max(n,N)} \mathbf{C}^{(i)} \right) \mathbf{T}, \quad (14)$$

and hence $\mathbf{T}^{(M)} = \mathbf{T}^{(N)}$ if $M > N$. \square

Therefore, if N is finite, we can compute the inverted light transport matrix \mathbf{T}^{-1} using Eq. 10. For example, from Eq. 10, the 2-bounce light transport is given by:

$$\mathbf{T}^{(2)} = (2\mathbf{I} - \mathbf{T}^{(1)}\mathbf{T}^{-1}) \mathbf{T}^{(1)}. \quad (15)$$

If the scene has only up to 2nd-bounce light, from Proposition 2 we have $\mathbf{T} = \mathbf{T}^{(2)}$. By substituting $\mathbf{T}^{(2)}$ with \mathbf{T} into Eq. 15, we obtain

$$\mathbf{T} = (2\mathbf{I} - \mathbf{T}^{(1)}\mathbf{T}^{-1}) \mathbf{T}^{(1)}. \quad (16)$$

Let's denote the inverse light transport matrix obtained by assuming the scene having up to i th bounce light as $\mathbf{T}^{(-i)}$. With a simple manipulation of Eq. 16, we obtain an expression for $\mathbf{T}^{(-2)}$:

$$\mathbf{T}^{(-2)} = \mathbf{T}^{(-1)} (2\mathbf{I} - \mathbf{T}\mathbf{T}^{(-1)}). \quad (17)$$

Similarly, for a scene with only up to 3rd-bounce light, we have:

$$\mathbf{T}^{(-3)} = \mathbf{T}^{(-1)} (\mathbf{T}\mathbf{T}^{(-1)} (\mathbf{T}\mathbf{T}^{(-1)} - 3\mathbf{I}) + 3\mathbf{I}). \quad (18)$$

For a scene with only up to 4th-bounce light, we have:

$$\mathbf{T}^{(-4)} = \mathbf{T}^{(-1)} (4\mathbf{I} - \mathbf{T}\mathbf{T}^{(-1)} (\mathbf{T}\mathbf{T}^{(-1)} (\mathbf{T}\mathbf{T}^{(-1)} - 4\mathbf{I}) + 6\mathbf{I})). \quad (19)$$

For a scene with only up to 5th-bounce light, we have:

$$\mathbf{T}^{(-5)} = \mathbf{T}^{(-1)} (5\mathbf{I} + \mathbf{T}\mathbf{T}^{(-1)} (\mathbf{T}\mathbf{T}^{(-1)} (\mathbf{T}\mathbf{T}^{(-1)} (\mathbf{T}\mathbf{T}^{(-1)} (\mathbf{T}\mathbf{T}^{(-1)} - 5\mathbf{I}) + 10\mathbf{I}) - 10\mathbf{I}))). \quad (20)$$

The similar technique can be used to derive any n -bounce stratified inverse light transport matrix $\mathbf{T}^{(-n)}$ with a recursive expression given by:

$$\begin{aligned}\mathbf{T}^{(-n)} = & (-1)^{n-1} \mathbf{T}^{(-1)} p \left(\dots p \left(p \left(\mathbf{I}, (-1)^1 \binom{n}{1} \right), (-1)^2 \binom{n}{2} \right) \right. \\ & \left. \dots, (-1)^{n-1} \binom{n}{n-1} \right),\end{aligned}\quad (21)$$

where $p(\mathbf{X}, a) = \mathbf{T} \mathbf{T}^{(-1)} \mathbf{X} + a \mathbf{I}$.

To compute $\mathbf{T}^{(-n)}$ in Eq. 21, we need to know $\mathbf{T}^{(1)}$ which is unobserved but can be approximated. In [8], a display constraint was introduced to simplify a light transport matrix by keeping only the largest element in each row. The simplified matrix is close to the 1-bounce transport matrix $\mathbf{T}^{(1)}$ if the first-bounce light transport mapping is one-to-one and no first-bounce light is weaker than non-first-bounce light. In this work, $\mathbf{T}^{(1)}$ is obtained by imposing the display constraint and it was shown in [8] that it is computationally simple to invert $\mathbf{T}^{(1)}$.

We can show the convergence of stratified inverses to the true inverse for the square matrix case as stated in Proposition 3. More details can be found in [5].

Proposition 3 (Convergence of Stratified Inverses). *When n increases, the stratified inverses converge to the true inverse of \mathbf{T} :*

$$\lim_{n \rightarrow \infty} \mathbf{T}^{(-n)} = \mathbf{T}^{-1},$$

if $\|\mathbf{I} - \mathbf{C}^{(-1)}\| < 1$ where $\mathbf{C}^{(-1)} = (\mathbf{C}^{(1)})^{-1}$

5. Simulations

In the first simulation, we assume that the number of projector pixels is the same as that of camera pixels, hence \mathbf{T} is a square matrix:

$$\mathbf{T} = \begin{pmatrix} 0.70 & 0.10 & 0.10 & 0.10 \\ 0.10 & 0.70 & 0.10 & 0.10 \\ 0.10 & 0.10 & 0.70 & 0.20 \\ 0.10 & 0.10 & 0.10 & 0.60 \end{pmatrix}. \quad (22)$$

We derive $\mathbf{T}^{(1)}$ from \mathbf{T} by keeping only the largest element in each row:

$$\mathbf{T}^{(1)} = \begin{pmatrix} 0.7 & 0.0 & 0.0 & 0.0 \\ 0.0 & 0.7 & 0.0 & 0.0 \\ 0.0 & 0.0 & 0.7 & 0.0 \\ 0.0 & 0.0 & 0.0 & 0.6 \end{pmatrix}. \quad (23)$$

We consider the direct inversion of \mathbf{T} , i.e., \mathbf{T}^{-1} , as the ground-truth for this simulation:

$$\mathbf{T}^{-1} = \begin{pmatrix} 1.50 & -0.17 & -0.17 & -0.17 \\ -0.17 & 1.50 & -0.17 & -0.17 \\ -0.13 & -0.13 & 1.53 & -0.47 \\ -0.20 & -0.20 & -0.20 & 1.80 \end{pmatrix}. \quad (24)$$

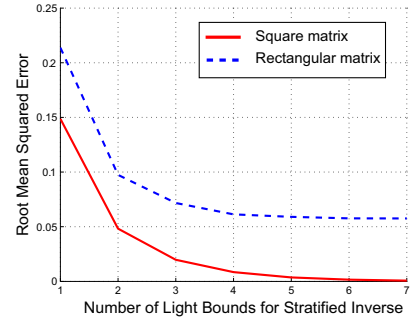


Figure 2. The RMSE of stratified inverses against the true inverse goes down as the number of light bound decreases.

We compute the stratified inverses as in Eq. 21. The 1-bounce inverse is just the inverse of $\mathbf{T}^{(1)}$ in Eq. 23. The 2-bound to 4-bound stratified inverses are given below:

$$\mathbf{T}^{(-2)} = \begin{pmatrix} 1.43 & -0.20 & -0.20 & -0.24 \\ -0.20 & 1.43 & -0.20 & -0.24 \\ -0.20 & -0.20 & 1.43 & -0.48 \\ -0.23 & -0.23 & -0.24 & 1.67 \end{pmatrix}, \quad (25)$$

$$\mathbf{T}^{(-3)} = \begin{pmatrix} 1.52 & -0.14 & -0.14 & -0.14 \\ -0.14 & 1.52 & -0.14 & -0.14 \\ -0.11 & -0.17 & 1.55 & -0.41 \\ -0.17 & -0.17 & -0.17 & 1.83 \end{pmatrix}, \text{ and} \quad (26)$$

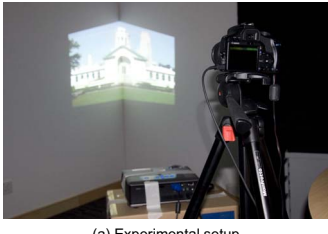
$$\mathbf{T}^{(-4)} = \begin{pmatrix} 1.49 & -0.18 & -0.18 & -0.18 \\ -0.18 & 1.49 & -0.18 & -0.18 \\ -0.14 & -0.19 & 1.52 & -0.48 \\ -0.21 & -0.21 & -0.21 & 1.78 \end{pmatrix}. \quad (27)$$

We can see that as the number of light bounces goes up, the elements of the stratified inverses oscillate around and converge to the ground-truth value in Eq. 24. The convergence toward the ground-truth is confirmed in Fig. 2 that the root-mean-squared error (RMSE) of stratified inverses decreases with the number of light bounces.

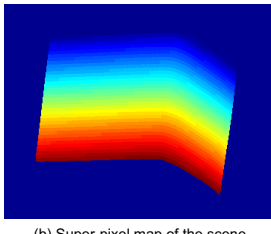
In the second simulation, we consider the case where the number of camera pixels is larger than that of projector pixels, where \mathbf{T} is a rectangular matrix:

$$\mathbf{T} = \begin{pmatrix} 0.6 & 0.1 & 0.1 & 0.1 \\ 0.1 & 0.6 & 0.1 & 0.1 \\ 0.1 & 0.1 & 0.6 & 0.1 \\ 0.1 & 0.1 & 0.1 & 0.5 \\ 0.1 & 0.1 & 0.1 & 0.2 \end{pmatrix}. \quad (28)$$

In this case, we consider the pseudo-inverse of \mathbf{T} as the ground-truth inverse. In Fig. 2, we observe that the RMSE of stratified inverses decreases with the number of light bounces although the error does not seem to converge to zero. Note that for the tall rectangular matrix case (i.e., $N_c > N_p$), the method in [8] corresponds to computing the 1-bound stratified inverse. Therefore, our method is a generalization of that in [8].



(a) Experimental setup



(b) Super-pixel map of the scene

Figure 3. (a) The experimental setup and the wall corner scene. (b) The super-pixel map on a camera image.

6. Experiments

As stratified inverses approximate the true inverse of a matrix and generalize the 1-bound inverse of [8], we validate their capability in compensating inter-reflection in a scene and compare their performance with that of the 1-bound inverse. The first scene for our experiment is a wall corner as shown in Fig. 3(a) which demonstrates a significant inter-reflection between two sides of the corner as seen in Fig. 4. For experimental setup, we used a Canon 450D camera and a Dell 2400MP projector as shown in Fig. 3(a). We linearized the system by first linearizing the camera using a Macbeth color checker and then linearizing the projector by projecting a sequence of grayscale images. In our experiment, we consider grayscale light transport for simplicity by assuming that the projector-camera color mixing matrix is diagonal.

For the first experiment, we focus on a small region centering at the wall corner. We group 4×4 projector pixels into a super-pixel and have 31×51 super-pixels on the projector. The corresponding super-pixel on the camera is a group of camera pixels that a projector super-pixel has the maximum response and the intensity of a camera superpixel is the mean of the group of camera pixels. The super-pixel map on a camera is shown in Fig. 3(b). With this setting, the light transport matrix \mathbf{T} is a square matrix of dimension 1938×1938 . There are many methods to acquire \mathbf{T} [7], we use a brute-force method for this experiment, as we turn on the projector super-pixel one by one and the recorded camera super-pixels form a column in \mathbf{T} .

We evaluate the quality of \mathbf{T} by comparing $\mathbf{c} = \mathbf{T}\mathbf{p}_{\text{const}}$ where $\mathbf{p}_{\text{const}}$ is a projector input image with constant intensity with the actual camera image when a constant-intensity image is projected by a projector. The horizontal scanlines of the two are shown in Fig. 4. We can see that the scanlines for the simulated \mathbf{c} and the actual \mathbf{c} are close in shape. The differences between them could be due to the deviation from the diagonal projector-camera color mixing matrix assumption. The scanlines also show the significant inter-reflection between the two sides of the wall corner.

We computed the 1-bounce to 4-bounce stratified inverses of \mathbf{T} as well as the actual inverse of \mathbf{T} . From Fig. 5(b), we can see that the stratified inverse computation is over 20 times more efficient than the true inverse

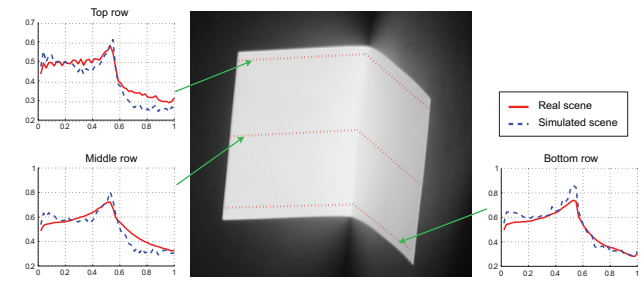


Figure 4. The projector output when projecting a constant-value image and three of its horizontal scanlines.

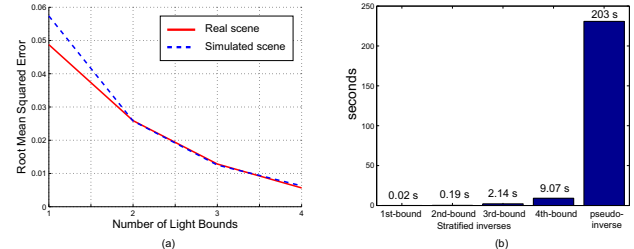


Figure 5. (a) The RMSE for the horizontal scanlines of both the simulated and captured $\mathbf{c}_{\text{actual}}$, for a constant-value $\mathbf{c}_{\text{desired}}$. (b) The time taken for computing the stratified inverses and the true inverse.

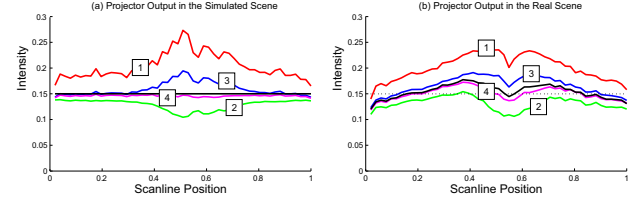


Figure 6. Results for the case of a constant-value $\mathbf{c}_{\text{desired}}$. (a) Horizontal scanlines for the simulated $\mathbf{c}_{\text{actual}}$. (b) Horizontal scanlines for the captured $\mathbf{c}_{\text{actual}}$. For both (a) and (b), the number i on the scanlines indicates i -bounce stratified inverse. The black-color scanline is one for the true inverse.

computation. The computational efficiency comes from the fact that the stratified inverse expression mainly involves matrix multiplication. To evaluate the capability of stratified inverses in undoing the inter-reflection in the scene, we specify $\mathbf{c}_{\text{desired}}$ as a constant-value image. We simulate $\mathbf{c}_{\text{actual}}$ according to Eq. 3 and also capture the projector output with $f_+(\mathbf{T}^{-1}\mathbf{c}_{\text{desired}})$ as the projector input, where $f_+(\cdot) = \max(\cdot, 0)$. A horizontal scanlines of the simulated $\mathbf{c}_{\text{actual}}$ and the captured $\mathbf{c}_{\text{actual}}$ are respectively shown in Fig. 6(a) and (b). Note that in both cases the scanlines for the stratified inverses approach that of the true inverse as the number of light bounces goes up, as also confirmed by their RMSE as shown in Fig. 5(a).

To visually evaluate the undoing of scene inter-reflection, Fig. 7 shows the captured $\mathbf{c}_{\text{actual}}$ as well as the corresponding projector inputs. We can see that comparing to the image from the 1-bound inverse, the image from the

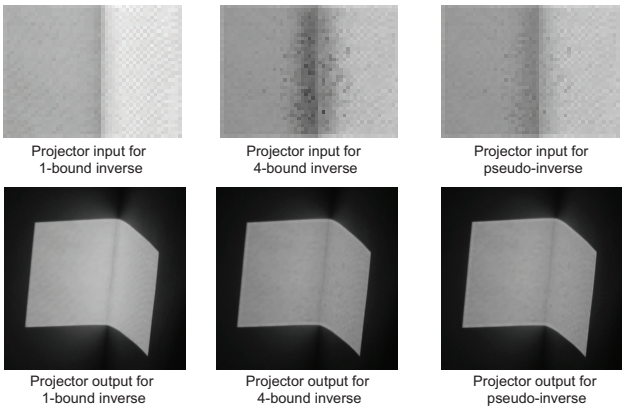


Figure 7. Results for the case of a constant-value c_{desired} . (Top row) The projector input for various inverses. (Bottom row) The projector output for various inverses.

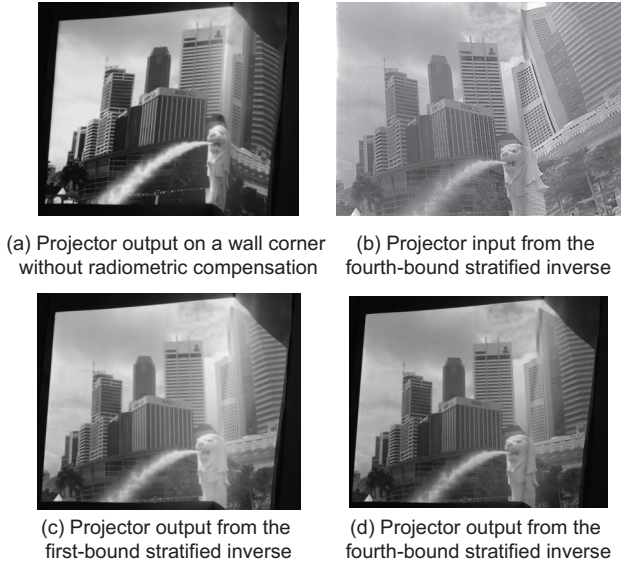


Figure 8. The high-resolution results for the wall corner scene.

4-bound inverse and that from the true inverse are close and have much less inter-reflection of light on the two walls. The dark line between the two walls is due to the fold at the wall corner. The dark line does not disappear at the compensated images because the sampling resolution of \mathbf{T} is not fine enough to capture the narrow fold at the wall corner.

To handle complex images, we acquire a high-resolution \mathbf{T} with the projector having 384×512 super-pixels of dimension 2×2 pixels. For efficiency, \mathbf{T} is acquired using the stripe method in [8], instead of the brute-force method. In this case, \mathbf{T} has a dimension of 196608×196608 . We specify c_{desired} as a city-scene image as shown in Fig. 8. Before radiometric compensation, the projector output is distorted. The compensation from both the 1-bound inverse and the 4-bound stratified inverse restores the image structure, but the scene inter-reflection of the latter is visibly much subdued.

For the second experiment, we choose a complex scene of a surface with a array of semi-spheres as shown in Fig. 1. The scene inter-reflection is significant and the projector output before compensation is seriously distorted. Similarly, we can see that the compensation from the 2-bound stratified inverse significantly reduces the scene inter-reflection and restore the image structure. Attempts in compensating for the shadow region results in white ring artifacts at some locations, which could be a form of over-compensation.

7. Conclusion

Radiometric compensation of a projector-camera system can be achieved through light transport matrix inversion, which is challenging for large matrices. We propose a principled way to quantify the tradeoff between accuracy and computational efficiency of inverse matrix computation, by stratifying the light transport of a scene. Through simulations and experiments, we showed that stratified inverses converge to the true inverse and is effective in undoing scene inter-reflection for radiometric compensation. Large matrix inversion is also crucial for other problems such as the Google page rank vector computation. In future work, we will find other applications for the stratified inverse framework.

References

- [1] O. Bimber, A. Emmerling, and T. Klemmer. Embedded Entertainment with Smart Projectors. *IEEE Computer Magazine*, 38(1):48–55, 2005.
- [2] Y. Ding, J. Xiao, K.-H. Tan, and J. Yu. Catadioptric Projectors. In *IEEE CVPR*, 2009.
- [3] K. Fujii, M. Grossberg, and S. Nayar. A Projector-camera System with Real-time Photometric Adaptation for Dynamic Environments. In *IEEE CVPR*, 2005.
- [4] S. Nayar, H. Peri, M. Grossberg, and P. Belhumeur. A Projection System with Radiometric Compensation for Screen Imperfections. In *IEEE International Workshop on Projector-Camera Systems*, 2003.
- [5] T.-T. Ng. homepage, <http://www1.i2r.a-star.edu.sg/~ttng/>.
- [6] S. Seitz, Y. Matsushita, and K. Kutulakos. A Theory of Inverse Light Transport. In *IEEE ICCV*, 2005.
- [7] P. Sen, B. Chen, G. Garg, S. Marschner, M. Horowitz, M. Levoy, and H. Lensch. Dual Photography. *ACM SIGGRAPH*, 2005.
- [8] K.-H. Tan and J. Xiao. View Projection: One-Touch Setup of Light Displays on Arbitrary Surfaces. *U.S. Patent Application 20080174704*, 2007.
- [9] G. Wetzstein and O. Bimber. Radiometric Compensation through Inverse Light Transport. In *Pacific Conference on Computer Graphics and Applications*, 2007.